Int. J. Electrochem. Sci., 12 **(2017)** 5964 – 5983, doi: 10.20964/2017.07.45

International Journal of
ELECTROCHEMICAL
SCIENCE
www.electrochemsci.org

Metronidazole Performance as Corrosion Inhibitor for Carbon Steel, 304L Stainless Steel and Aluminum in Hydrochloric Acid Solution

Adriana Samide[1,*], *Petru Ilea*[2], *Ana-Cristina Vladu*[1,2]

[1] University of Craiova, Faculty of Sciences, Department of Chemistry, Calea Bucuresti 107i, Craiova, Dolj, Romania
[2] Babes-Bolyai University, Faculty of Chemistry and Chemical Engineering, Arany Janos Street, no. 11, Cluj-Napoca, Romania
[*]E-mail: samide_adriana@yahoo.com

Received: 21 March 2017 / *Accepted:* 5 May 2017 / *Published:* 12 June 2017

The purpose of this paper is to study a possibility of reintroduction in circulation of the expired drugs, as ecological corrosion inhibitors that can have a decisive effect on decreasing of metallic corrosion rate. In this regard, we simultaneously present an overview on metronidazole drug performance, as corrosion inhibitor of three substrates in hydrochloric acid solution. The electrochemical measurements such as potentiodynamic polarization and electrochemical impedance spectroscopy were performed to determine the metronidazole inhibition efficiency that has reached the highest level for aluminum, followed by carbon steel and 304L stainless steel. To discuss the metronidazole action mechanism, UV-Vis spectrophotometry was applied to analyze the uninhibited and inhibited solutions, this showing that in the absence of metronidazole, the solutions were infested with higher amount of metal cations compared to those were inhibited with metronidazole. Corroborating the information, it can affirm that, the protective coatings were formed by overlapping of some processes like pure adsorption of metronidazole and electrostatic interactions for aluminum and, complementary for steels, the adsorption of their complexes with iron, helpful supports being El-Awady kinetic model and Temkin adsorption isotherm, respectively.

Keywords: corrosion inhibition; electrochemical measurements; metronidazole; carbon steel; stainless steel; aluminum

1. INTRODUCTION

The corrosion is a major topic of research aimed at implementation of appropriate methods for the protection of metal surfaces to prevent their irreversible degradation. In contact with aggressive

media, the metals/alloys are damaged by oxidation processes, their surface being fully or partially affected. Also, the corrosion can deeply penetrate, causing extensive cracks or cavities. Thus, certain properties of the metal are changed, and the resulted corrosion products migrate into the environment, leading to the pollution and the alteration of its qualities like appearance.

The studies have shown that certain organic substances, which contain sulfur, oxygen and nitrogen atoms in their molecule, have been proposed as corrosion inhibitors, in order to improve the characteristics of the metal/alloy. Most of the organic substances act by adsorption, forming inhibitory layers which restrict the corrosion processes [1-12]. The effectiveness of inhibition depends on the environment nature and pH, temperature, the type and the concentration of organic compounds [7-11].

The selection of the corrosion inhibitors has as basic aim the replacement of toxic substances with other ecological compounds, developing the concept of "Green Chemistry" in the corrosion inhibition field. Thus, the reintroduction in current stage of expired drugs was a plausible reason for their investigation as corrosion inhibitors [9, 12-20].

The corrosion inhibition of carbon steel, stainless steel and aluminum, mostly in acid solutions, has been the topic of many researches due to their numerous industrial applications. It is known that the carbon steel is corroded in acid media with appreciable rate, while 304L type has a higher susceptibility to corrosion compared to other stainless steels [20]. The oxide film formed on the aluminum surface increases the corrosion resistance, but the amphoteric feature of oxide coating leads to its significantly dissolution when the contact between this metal and solution of acids or bases takes place [21]. These are the specific reasons of the extensive research on corrosion inhibition of carbon steel, 304L stainless steel and aluminum in acid media being reported a wide series of compounds which behave as inhibitors [1-30], including the action of drugs on the surface of: carbon/mild steel [9, 12-19, 22-24], 304L/316L stainless steel [20, 25, 26] and aluminum [27-30].

To investigate the performance of some compounds as corrosion inhibitors in presence of Cl^- ions the weight loss and electrochemical measurements [31-34, 37-46] were successfully performed for carbon steel, stainless steel and aluminum followed by some associative methods, such as: scanning electron microscopy (SEM) [37-43] optical microscopy [6, 9, 40], X-ray photoelectron spectroscopy (XPS) [9] and UV-Vis spectrophotometry [9, 40, 42], etc.

In order to propose an action mechanism of corrosion inhibitors and to discuss the adsorption type, several studies have reported a way to fit the experimental data according to the specific adsorption isotherms: Langmuir [31, 37, 39, 44-46], Temkin [32, 41, 42], Freundlich [40] and El-Awady kinetic-thermodynamic model [46].

The current study reports the performance of metronidazole, IUPAC name: 2-(2-methyl-5-nitroimidazol-1-yl) ethanol, as corrosion inhibitor for carbon steel, 304L stainless steel and aluminum in 1.0 mol L^{-1} HCl solution. Metronidazole (MNZ) is an antibiotic and antiparasitary drug used for the treatment of abdominal inflammatory disease [33]. The electrochemical measurements performed on all substrates in 1.0 mol L^{-1} HCl solution, without and with MNZ, have been accompanied by the UV-Vis spectrophotometry of uninhibited and inhibited solutions, before and after corrosion. Based on literature data and our experiments, the MNZ action mechanism was proposed and all results were comparatively presented for the three investigated materials, achieving an overview on their behaviour in uninhibited and inhibited acid media. Thus, two objectives can be achieved, like the decline in

deterioration process of metals/alloys and consequently, the prevention of the medium pollution with corrosion products, using friendly environmental compounds, with minimum impact on human health.

2. MATERIALS AND METHODS

2.1. Materials

The sheets of materials, with an active area of 1.0 cm^2 were submitted to corrosion, at room temperature and static regime, in 1.0 mol L^{-1} HCl blank solution and 1.0 mol L^{-1} HCl blank solution containing various concentrations of MNZ: 0.2 mmol L^{-1}; 0.4 mmol L^{-1}; 0.6 mmol L^{-1}; 0.8 mmol L^{-1}. The studied materials have the following composition: high-purity aluminum of 99.99 % from Sigma Aldrich; 304L stainless steel (alloy: FeNi18Cr10) from Sigma Aldrich containing (wt %): C-0.03; Ni-18; Cr-10 %; Mn-2.0 %; Fe balance; low carbon steel from O'Neal Steel having (wt %): carbon between 0.05-0.25 % ; up to 0.4 % manganese; the amount of other elements does not exceed 2.0 %; Fe remainder up to 100 %. Both, MNZ drug powder and HCl of analytical purity degree were purchased from Merck. The above mentioned solutions were prepared with bi-distillated water. Before corrosion, the samples were mechanically polished with emery paper, degreased with acetone and dried between two sheets of filter paper.

2.2. Electrochemical measurements

Both the potentiodynamic polarization and the electrochemical impedance spectroscopy (EIS) were performed using an electrochemical system constituted by a potentiostat/galvanostat VoltaLab 40, with VoltaMaster 4 software and a standard electrochemical cell containing the corrosion media in which three electrodes were immersed as follows: the working electrode manufactured from investigated substrate, a platinum plate as auxiliary electrode, their active area being of 1.0 cm^2 and Ag/AgCl electrode as reference. All measurements were accomplished at room temperature, after a relaxation time of the electrodes at open circuit of 4 minutes, when the scanned potential at open circuit was stabilized.

The potentiodynamic polarization were conducted, with a potential scan rate of 1.0 mV s^{-1}, in potential range from -1.0 V to -0.2 V for both carbon and stainless steel and from -1.6 V to -0.2 V for aluminum. The potentiodynamic curves were processed as Tafel diagrams in potential range of ± 200 mV around corrosion potential values.

The electrochemical impedance spectroscopy was carried out, at open circuit, in the frequency range of 10^5 Hz and 10^{-1} Hz, with an AC perturbation signal of 10 mV.

2.3. UV-Vis spectrophotometry

In order to discuss the composition change of corrosive solutions after potentiodynamic polarization applied on all substrates mentioned above, UV-Vis spectrophotometry was used for

analysis of 1.0 mol L^{-1} HCl blank solution and 1.0 mol L^{-1} HCl solution containing 0.2 mmol L^{-1} MNZ and 0.4 mmol L^{-1} MNZ, the last two accurately showing the MNZ peak on absorbance scale, compared to those that contained a higher concentration of metronidazole.

The UV-Vis spectra in wavelength range between 500 and 200 nm were recorded using an UV-Vis Varian-Cary 50 spectrophotometer with CaryWin software. Therefore, the absorbance maxima for specific corrosion products and MNZ were evidenced.

3. RESULTS AND DISCUSSION

3.1. Potentiodynamic polarization and UV-Vis spectrophotometry

The electrochemical performance of MNZ as corrosion inhibitor for carbon steel, 304L stainless steel and aluminum was discussed according to the results obtained from potentiodynamic polarization associated with UV-Vis spectrophotometry. The potentiodynamic curves processed as Tafel diagrams are presented in Figs. 1a, 2a and 3a. The inhibitor addition in the corrosive environment has a specific influence on each substrate, involving the differences between the characteristics of potentiodynamic curves and their shifting compared to that was recorded in the control solution.

As shown Fig. 1a, the carbon steel corrosion inhibition is very nuanced starting with the MNZ concentration value of 0.2 mmol L^{-1} up to 0.8 mmol L^{-1}, this being explained by the displacement of polarization curves recorded for carbon steel in inhibited media towards current density lower areas than that obtained in the blank solution.

Consequently, the corrosion current density (i_{corr}) decreases proportionally with the MNZ concentration. The corrosion potential (E_{corr}) is slightly shifted to positive direction excepting the first solution, MNZ acting on both anodic and cathodic processes, with the evident effect of the increase of its concentration on the metallic oxidation. Thus, MNZ acts as mixed corrosion inhibitor for carbon steel in 1.0 mol L^{-1} HCl solution, the hydrogen evolution reaction being less dependent of its concentration than the oxidation reaction. The phenomena above described may be associated with the development of a surface anodic film [31] that inhibits the corrosion of carbon steel in 1.0 mol L^{-1} HCl solution, implying the adsorption of the inhibitive species on the electrode surface [32, 33]. The investigation of UV-Vis spectra (Fig. 1b) recorded before and after the corrosion of carbon steel in 1.0 mol L^{-1} HCl blank solution and in 1.0 mol L^{-1} HCl solution containing 0.2 mmol L^{-1} and 0.4 mmol L^{-1} MNZ leads to the following observations: (i) the spectrophotometric analysis of 1.0 mol L^{-1} HCl blank solution, after corrosion, shows a peak at λ_{max} = 331 nm; this can be attributed to Fe^{2+} species formed in the absence of inhibitor [34]; (ii) in the spectra of inhibited solutions it can be observed, a sharp peak at λ_{max} = 277 nm corresponding to MNZ, that is in good agreement with the literature data [35]; (iii) after corrosion, the spectral analysis of inhibited solution, shows that the characteristics and intensity of MNZ peaks are changed, without the altering the λ_{max} value, this being due to the interactions between MNZ and Fe^{2+}, with the formation of complexes [35, 36]; these are interposed at metal/electrolyte interface leading to the development of the protective layer on the carbon steel surface; moreover, the peak intensity of Fe^{2+} considerable decreases compared to that was scanned for

the uninhibited solution, indicating that MNZ slows down the iron oxidation, consequently the corrosion of carbon steel in 1.0 mol L^{-1} HCl solution.

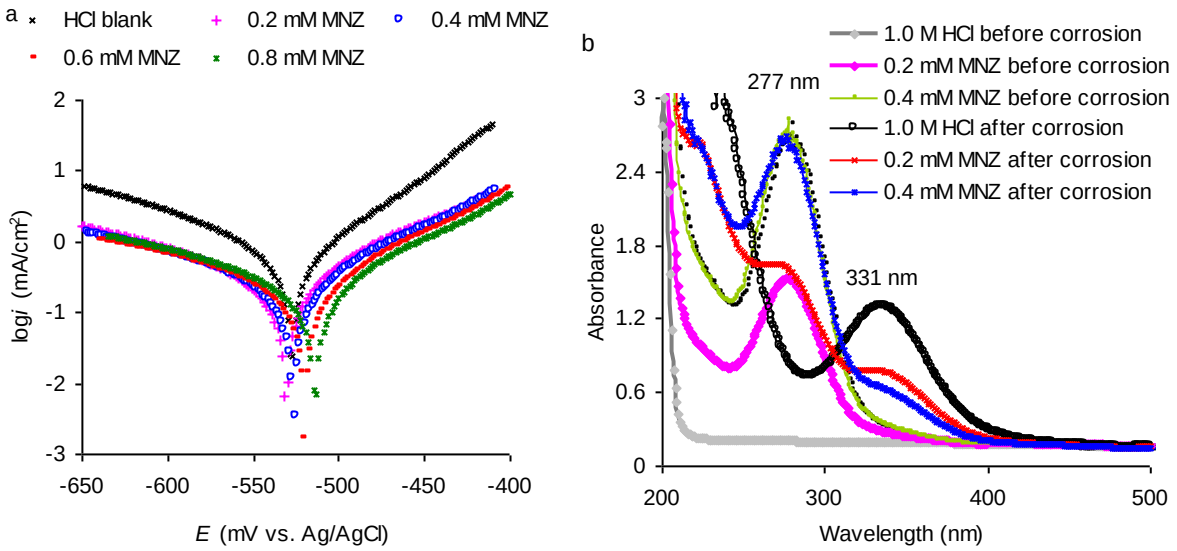

Figure 1. The results obtained for carbon steel before and after corrosion in 1.0 mol L^{-1} HCl solution without and with MNZ inhibitor: a – potentiodynamic curves; b – UV-Vis spectra recorded for 1.0 mol L^{-1} HCl solution in the absence of MNZ and in 1.0 mol L^{-1} HCl solution containing 0.2 mmol L^{-1} MNZ and 0.4 mmol L^{-1} MNZ

If in the case of carbon steel is obvious the MNZ inhibitory action on both, anodic and cathodic processes (Fig. 1a), on the contrary for the 304L stainless steel corrosion, the addition of inhibitor in 1.0 mol L^{-1} HCl solution leads to the E_{corr} movement in positive direction more perceptible, affecting in upper manner the oxidation than the hydrogen evolution reaction (Fig. 2a).

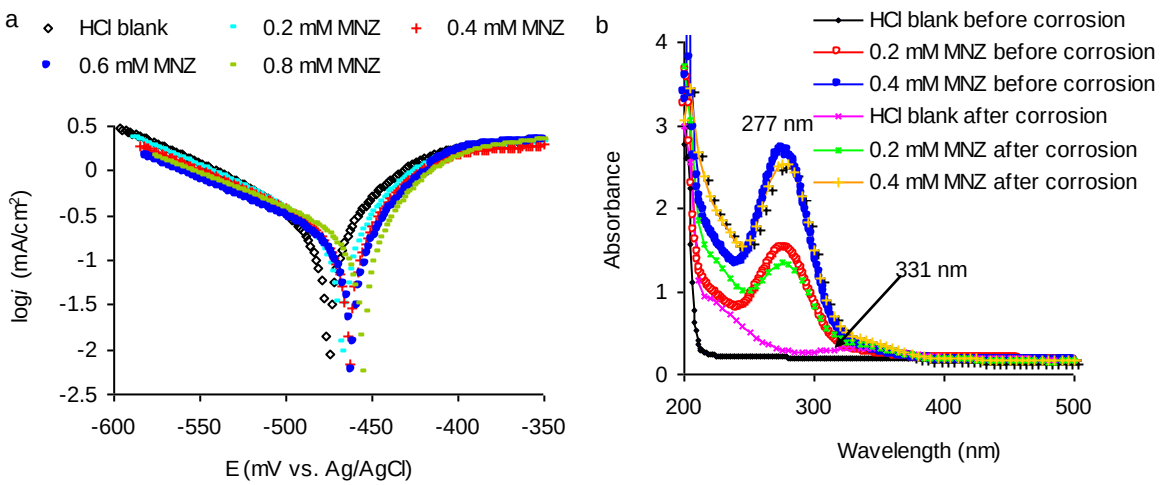

Figure 2. The results obtained for 304L stainless steel before and after corrosion in 1.0 mol L^{-1} HCl solution without and with MNZ inhibitor: a - potentiodynamic curves; b - UV-Vis spectra recorded for 1.0 mol L^{-1} HCl solution in the absence of MNZ and in 1.0 mol L^{-1} HCl solution containing 0.2 mmol L^{-1} and 0.4 mmol L^{-1} MNZ

Analyzing the cathodic process (Fig. 2a), it can be commented that the polarization curves, in the presence of inhibitor, overlap on that one was recorded, in the absence of inhibitor. Thus, at the potential value lower than -0.500 V, straight lines were obtained, indicating that the process is theoretically controlled by the cathodic Tafel equation. In contrast, in the anodic process case, for all concentrations of inhibitor, the polarization curves were gradually shifted in positive direction until the potential -389.5 mV vs. Ag/AgCl. At the potentials higher than -389.5 mV vs. Ag/AgCl, these are overlapped on that one that obtained in blank solution, the inhibition being mitigated and the oxidation prevails. Consequently, MNZ is a mixed type of inhibitor for 304L stainless, with an obvious anodic predominance, unlike carbon steel, when both processes are suppressed by MNZ, but the cathodic process is less influenced by its concentration. The UV-Vis different spectrum from that of carbon steel was registered, it indicating a much lower amount of metal ions in uninhibited solution, what was expected knowing that the stainless steel is less susceptible to corrosion. Moreover, the literature data have shown that the passivation process can take place [37] by the oxyhydroxides film formation [37] and the occurrence of some adsorbed species, such as: $(FeCl)_{ads}$, $(CrCl)_{ads}$ and $(NiCl)_{ads}$ on stainless steel surface, in the potential range of -800 to -200 mV was reported [37]. By the oxidation, these remit in electrolyte the corresponding ions: Fe^{2+}, Cr^{3+} and Ni^{2+}, respectively. The complexes formation between Fe^{2+} and MNZ [35, 36] may be revealed by the MNZ scans after corrosion, when the allure of the peak is slightly changed and the intensity of absorbance maximum slowly decreases compared to carbon steel.

However, a competitive process of MNZ pure adsorption can not be excluded, even more as the decreasing of the adsorption maximum intensity may be an effect of this assumption, especially for 304L stainless steel when the amount of Fe^{2+} ions from solution is greatly diminished and the characteristic peaks of MNZ are minimally altered compared to carbon steel (Figs. 1b and 2b).

Consequently, both for carbon steel corrosion as well as the 304L stainless steel corrosion in 1.0 mol L^{-1} HCl solution containing MNZ, the initiation of anodic film formation may be discussed according to the pure adsorption of inhibitor on the substrates, that takes place especially at open circuit, it being followed by the anchoring of MNZ-iron (II) complexes on the metallic surfaces, having a conclusive effect on the development and completion of the protective layer.

Completely different, the aluminum behaves in 1.0 mol L^{-1} HCl solution, in the presence of MNZ. The potentiodynamic curves illustrated in Fig. 3a shows that the presence of inhibitor leads to significant shifting of the polarization curves towards higher potential values and in lower areas of current density, suggesting that the corrosion current density decreases while the MNZ concentration increases. By immersing the aluminum in 1.0 mol L^{-1} HCl solution the oxide film spontaneously formed on aluminum surface is dissolved [38, 39], the dissolution rate is greater than its formation rate [38] being facilitated the Al oxidation followed by the release of its ions in electrolyte [38, 39].

As seen in Fig. 3a, in the presence of MNZ, the anodic polarization curves have shifted to much lower current areas compared to the cathodic ones. Moreover, starting with 0.2 mmol L^{-1} MNZ and ending with 0.6 mmol L^{-1} MNZ, at potential values lower than -1.0 V vs. Ag/AgCl, the polarization curves overlap with that obtained in the blank solution, the cathodic process being mainly affected on the entire range of potential, only for a MNZ concentration of 0.8 mmol L^{-1}. Thus, the

reaction of hydrogen evolution is dependent on the MNZ concentration, seeing a sharp decline of the cathodic current densities, at the inhibitor concentration of 0.8 mmol L^{-1}.

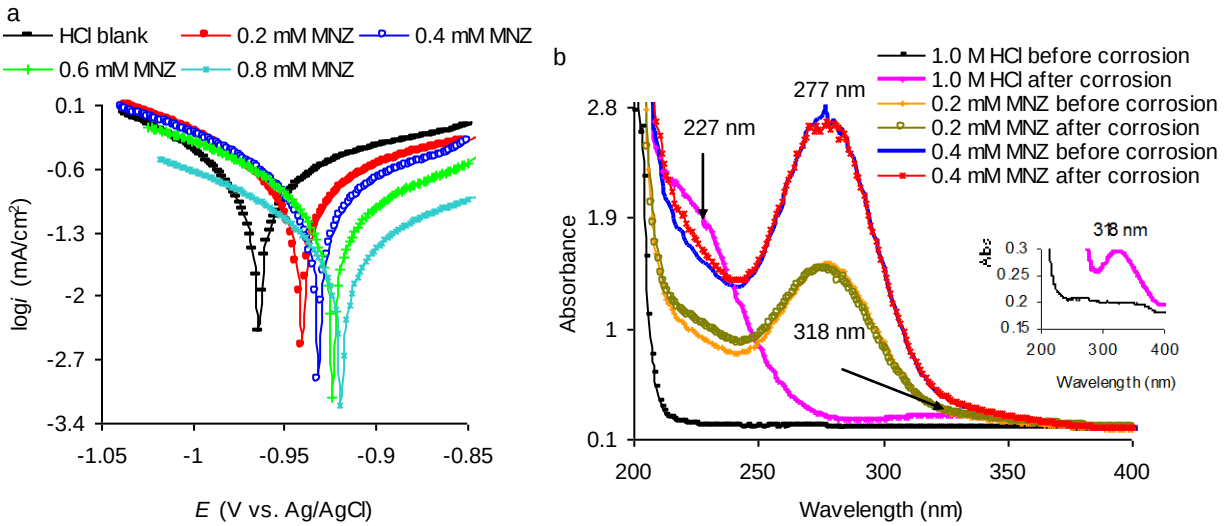

Figure 3. The results obtained for aluminum before and after corrosion in 1.0 mol L^{-1} HCl solution without and with MNZ inhibitor: a – potentiodynamic curves; b – UV-Vis spectra recorded for 1.0 mol L^{-1} HCl solution in the absence of MNZ and in 1.0 mol L^{-1} HCl solution containing 0.2 mmol L^{-1} MNZ and 0.4 mmol L^{-1} MNZ

Clearly, the MNZ presence in 1.0 mol L^{-1} HCl solution causes the changing both, the shape as well as the position of the anodic polarization curves, suggesting that the blocking of electron transfer reactions takes place by the anodic protective film formation on the aluminum surface [38, 39]. Therefore, MNZ acts as a mixed inhibitor for aluminum corrosion in 1.0 mol L^{-1} HCl solution, being greatly affected both processes. Those aforementioned are supported by spectrophotometric analysis performed before and after corrosion for the 1.0 mol L^{-1} HCl blank solution and 1.0 mol L^{-1} HCl solution containing 0.2 mmol L^{-1} MNZ and 0.4 mmol L^{-1} MNZ, respectively (Fig. 3b). Two adsorption maximum, at 318 nm and 227 nm, may be observed for HCl blank solution, being attributed to the Al^{3+} species released in electrolyte after aluminum corrosion. The UV-Vis spectra of MNZ solution, after corrosion, are almost identical to those obtained before corrosion. The absorbance maximum value is really easy modified due to the MNZ adsorption on aluminum surface. It can conclude that MNZ is an inhibitor for aluminum corrosion in 1.0 mol L^{-1} HCl solution, acting by adsorption on surface, merely blocking the active sites.

According to potentiodynamic measurements, UV-Vis spectrophotometry and based on literature data [31-42] the following conclusions can be formulated: (i) MNZ acts as mixed corrosion inhibitor for those three substrates, anodic preponderance being more nuanced for 304L stainless steel and aluminum; (ii) MNZ action is based on complexes formation with Fe^{2+} that prevails the pure adsorption for carbon steel corrosion inhibition, but this being the competitive process for corrosion inhibition of 304L stainless steel, in contrast to aluminum corrosion inhibition that is due to MNZ pure adsorption on the surface.

For all substrates corroded in 1.0 mol L^{-1} HCl solution, in the absence and in the presence of MNZ, the electrochemical parameters such as: corrosion potential (E_{corr}), corrosion current density (i_{corr}), polarization resistance (R_p) anodic and cathodic Tafel slopes (b_a and b_c) were determined using the VoltaMaster 4 software; the corrosion current density was obtained at intersection of anodic and cathodic Tafel lines extrapolated to corrosion potential, subsequently its value being converted to corrosion rate (*CR*) using the same software. The corrosion current density (i_{corr}), polarization resistance (R_p) and corrosion rate (*CR*) were used, in order to calculate the inhibition efficiency (*IE*/%) of MNZ on corrosion of carbon steel, 304L stainless steel and aluminum in acidic solution taking into consideration the following equations, Eqs. 1, 2 and 3 [31, 32, 37-46]:

$$IE = \frac{i^{o}_{corr} - i_{corr}}{i^{o}_{corr}} \times 100 \quad (1)$$

$$IE = \frac{R_p - R^{o}_p}{R_p} \times 100 \quad (2)$$

$$IE = \frac{CR^{o} - CR}{CR^{o}} \times 100 \quad (3)$$

where: i^{o}_{corr}, R^{o}_p, CR^{o} represent the corrosion current density, polarization resistance and corrosion rate (μm/year) obtained for the corrosion of substrates in 1.0 mol L^{-1} HCl blank solution; i_{corr}, R_p and *CR* represent the corrosion current density, polarization resistance and corrosion rate (μm/year) obtained for the corrosion of substrates in 1.0 mmol L^{-1} HCl containing various MNZ concentrations. The Table 1 centralizes all these results.

By data analyzing listed in Table 1, it can conclude that: (i) in all corrosion cases, i_{corr} and *CR* decreased, while R_p and *IE* increased with the increase in MNZ concentration; at MNZ concentration value of 0.8 mmol L^{-1}, the *IE* reached a higher level for the aluminum (about 91.0%), followed by the carbon steel (approximately 81.0 %) and finally for 304L stainless steel, nearly 69.0% was obtained; (ii) the Tafel slopes are specific to each substrates and their values distinctive vary, as follows: for carbon steel, b_a has the values between 77±8 mV/dec while b_c varies betwen 155±18 mV/dec; the corrosion of 304L stainless steel is characterized by: b_a of 65±12 mV/dec and b_c of 128±8 mV/dec; aluminum Tafel slopes are included: b_a in the interval of 295±36 mV/dec and b_c covers the range of 120±25 mV/dec; thus, in all cases of substrates subjected to corrosion in 1.0 mol L^{-1} HCl solution without and with MNZ, the variation of Tafel slopes falls into an acceptable range, suggesting that the addition of inhibitor in the acid solution does not change the corrosion mechanism and the inhibition manifests by blocking the active sites on surface *via* the compounds which form the adsorbed protective layer [40-42, 44-47]. Similar behaviour was reported for other drugs used as corrosion inhibitors in the presence of Cl^- ions for carbon steel [32, 40-42, 48-50], stainless steel [37, 46, 51, 52] and aluminum [39, 45, 53].

Table 1. Inhibition efficiency (*IE*/%), corrosion rate (*CR*-μm/year) and the electrochemical parameters calculated from poteniodynamic polarization performed for carbon steel, 304L stainless steel and aluminum in 1.0 mol L^{-1} HCl solution, in the absence and in the presence of MNZ, at room temperature

C-MNZ/ mmol L^{-1}	E_{corr}/ mV vs. Ag/AgCl	i_{corr}/ μA cm^{-2}	b_a/ mV dec^{-1}	b_c/ mV dec^{-1}	CR/ μm $year^{-1}$	R_p/ Ω cm^2	*IE*/ %		
							from i_{corr}	from R_p	from CR
Carbon steel									
0	-527.8	839.0	68.9	-136.7	9572.0	15.3	-	-	-
0.2	-530.9	387.0	75.6	-157.8	4539.9	33.1	55.4	53.7	52.6
0.4	-525.9	254.0	78.4	-146.3	2979.7	50.4	69.7	69.6	68.9
0.6	-521.0	198.0	85.1	-163.3	2323.8	67.7	76.4	77.4	75.7
0.8	-514.0	163.0	81.2	-173.6	1912.2	80.6	80.6	81.1	80.0
304L Stainless steel									
0	-475.6	289.6	78.9	-134.0	3397.0	44.2	-	-	-
0.2	-468.2	207.8	68.3	-118.9	2439.2	61.8	28.2	28.5	28.2
0.4	-463.6	143.2	62.2	-123.5	1678.1	87.4	50.6	49.4	50.6
0.6	-461.1	123.7	58.3	-123.9	1451.2	102.5	57.3	56.9	57.2
0.8	-455.5	93.1	52.8	-121.0	1089.7	139.5	67.9	68.3	67.9
Aluminum									
0	-964.5	317.5	331.3	-144.3	3455.0	30.2	-	-	-
0.2	-940.5	230.1	303.1	-138.6	2535.0	47.9	27.5	36.9	26.6
0.4	-931.5	115.4	254.9	-141.1	1271.6	141.3	63.7	78.6	63.2
0.6	-924.0	70.3	256.2	-104.9	774.6	269.1	77.8	88.7	77.5
0.8	-919.5	37.4	259.4	-94.9	403.6	338.5	88.2	91.1	88.3

3.2. Electrochemical impedance spectroscopy

The electrochemical impedance spectroscopy was performed for all substrates in the frequency range between 10^5 Hz and 10^{-1} Hz, at their open circuit potential, the relaxation time of the electrodes being of 4.0 min., at room temperature. The Nyquist and Bode diagrams were recorded in order to discuss the behaviour of carbon steel, 304L stainless steel and aluminum in 1.0 mol L^{-1} HCl solution, in the absence and in the presence of MNZ. These are shown in Figs. 4, 5 and 6, where the equivalent circuit that the best fits the experimental data was inserted. From the Nyquist diagrams (Figs. 4a, 5a and 6a) the following motivations are deducted which support the MNZ behavior as inhibitor in the acid environment for the corrosion of investigated substrates: (1) the capacitive loops, with a nearly semicircular shape were obtained; the diameters are getting larger as the MNZ concentration increases; (2) considering that there is a direct proportional relationship between the semicircle diameter and the corrosion resistance, it can be asserted that with the increasing of MNZ concentration, the corrosion susceptibility of the carbon steel [31, 34, 39, 55, 56], the 304L stainless steel [44, 46, 52] and the aluminum [38, 47, 53, 54] decreases.

The easiest way of experimental data fitting is represent by Randles equivalent circuit (inserted in Figs. 4a, 5a and 6a) [31, 34, 38, 44, 46, 47, 52-56] which involves a parallel position between

charge-transfer resistance (R_{ct}) and constant phase element (*CPE*), both being connected in series with solution resistance (R_s). The intersection of the capacitive loop with the real axis represents: at very low frequencies charge-transfer resistance (R_{ct}) and the electrolytic resistance (R_s) at very high frequencies [31]. The imperfections of the surface and their effect are simulated by *CPE* [47]. The *CPE* impedance (Z_{CPE}) was be determined with the Eq. 4 [55, 57, 58]:

$$Z_{CPE} = \frac{1}{T(j\omega)^n} \quad (4)$$

where T is a proportional factor, j equals −1, ω is the angular frequency and n is the phase shift, between 0 and 1, describing the constant phase angle of the *CPE*. For n = 0, Z_{CPE} represents a resistance with $R = T^{-1}$; for n = 1, Z_{CPE} is a capacitance with $C = T$. When n is close near 1.0, the *CPE* obeys the capacitive behavior, as shown in Table 2.

The imperfect semicircle shapes can be observed in Nyquist diagrams (Figs. 4a, 5a and 6a), followed by one phase maximum in corresponding Bode chart (Figs. 4b, 5b and 6b).

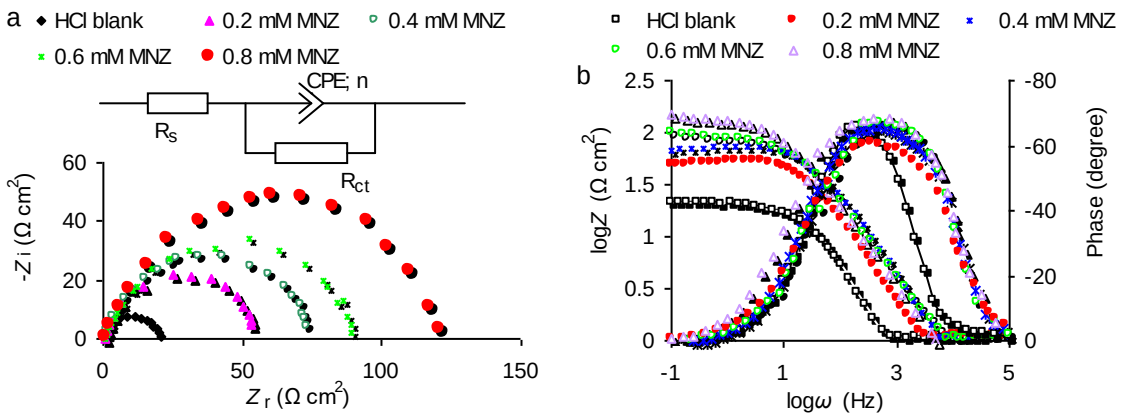

Figure 4. Nyquist and Bode diagrams recorded for carbon steel corroded in 1.0 mol L^{-1} HCl solution without and with various concentrations of MNZ, at room temperature

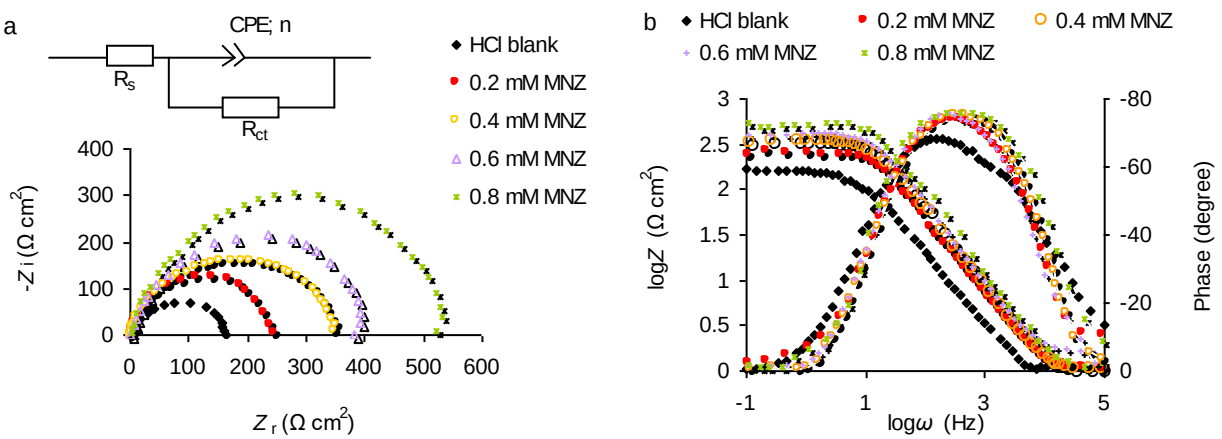

Figure 5. Nyquist and Bode diagrams recorded for 304L stainless steel corroded in 1.0 mol L^{-1} HCl solution without and with various concentrations of MNZ, at room temperature

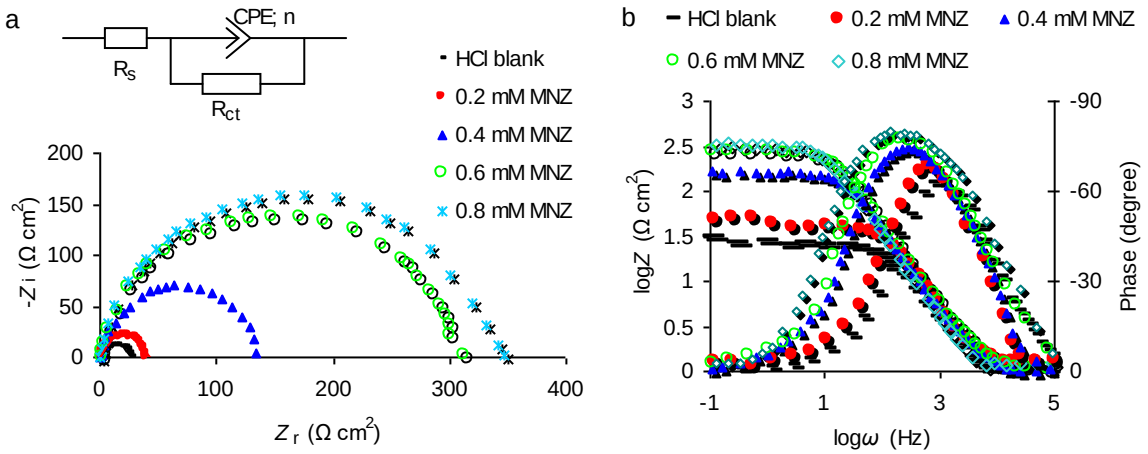

Figure 6. Nyquist and Bode diagrams recorded for aluminum corroded in 1.0 mol L^{-1} HCl solution without and with various concentrations of MNZ, at room temperature

Authors as B. Zerga et al. [31] reported similar behaviour of carbon steel corroded in HCl solution in the absence and in the presence of some tripodal bipyrazolic compounds, commenting this as result of the non-homogeneity or the roughness of the solid state [31]. The same trend, as illustrated in Figs. 4a and 4b was also described by Nazeer et al. [49, 55] for cefazolin and cefotaxime as corrosion inhibitors for carbon steel in H_2SO_4 solution [49] and for cefoperazone in HCI solution [55], concluding that the corrosion is mainly controlled by charge-transfer [49, 55]. The effect of some antibacterial drugs on the corrosion behavior of stainless steel type 304 in 1.0 mol L^{-1} HCl solution has been studied by Fouda et. al [46], recording a single capacitive loop in Nyquist diagram, both in uninhibited and inhibited solutions [46]. The Bode plot explicitly showed that the phase angle has not reached 90° [46] as it would for pure capacitive impedance [46], this being in good agreement with our results (Figs. 5a and 5b). Caliskan and Akbas [44] showed that the depressed semicircles in Nyquist diagram were recorded for the stainless steel corroded in 1.0 mol L^{-1} HCl solution without and with pyrimidine derivatives [44], indicating that the double layer on the material/solution interface has not acted as an ideal capacitor [44], this being modeled as the constant phase element (*CPE*) [44], as shown, also, in our study. Similar results reflected in or study *via* Fig. 6 were obtained by Bhat and Alva [54] for the investigation of the meclizine hydrochloride inhibition effect on the corrosion behaviour of aluminum in 1.0 mol L^{-1} HCl [54], as well as Abdallah and Jahdaly [53] for the performance of gentamicin, kanamycin and amikacin drugs as corrosion inhibitors of aluminum in 1.0 HCl solution [53].

The MNZ inhibition efficiency (*IE*) was calculated for the three materials corroded in 1.0 mol L^{-1} HCl solution as a function of charge-transfer resistance (R_{ct}) using the equation presented below (Eq.5), it being specified for carbon steel [31, 49, 55], stainless steel [44, 46] and aluminum [53, 54]:

$$IE = \frac{R_{ct} - R^{o}_{ct}}{R_{ct}} \times 100 \qquad (5)$$

where R^{o}_{ct} and R_{ct} represent the charge-transfer resistance obtained for the corrosion of the materials in 1.0 mol L^{-1} HCl without and with MNZ, respectively.

The solution resistance (R_s), the double-layer capacitance (C_{dl}) and the charge-transfer resistance (R_{ct}) were determined with VoltaMaster software. These are listed in Table 2, as well as *IE*.

The impedance data presented in Table 2 lead to the following conclusions regarding the behaviour of carbon steel, 304L stainless steel and aluminum in uninhibited and inhibited 1.0 mol L^{-1} HCl solution: (i) with the increase in MNZ concentration R_{ct} reached the higher values while for C_{dl} a lower levels were determined; (ii) the data obtained for Bode diagram like log*Z* show that the responses of impedance, at lowest frequency, increases with inhibitor concentration; (iii) the corroboration of collected data from Nyquist and Bode diagrams leads to the assumption that, the inhibiting effect of MNZ can be attributed to its specific adsorption at the material/solution interface [46, 49]; (iii) the increase in inhibition efficiency (*IE*) was obtained, it having a directly proportional dependence over MNZ concentration; (iv) the values of inhibition efficiency (*IE*) are very close to those achieved from potentiodynamic polarization, as follows: aluminum (91.7 vs. about 91.0 %), the next being the carbon steel (83.3 % vs. approximately 81.0 %) and finally for 304L stainless steel 69.8 % vs. nearly 69.0 %, it was obtained.

Table 2. Inhibition efficiency (*IE*/%) and electrochemical parameters calculated from EIS measurements performed for carbon steel, 304L stainless steel and aluminum in 1.0 mol L^{-1} HCl solution, in the absence and in the presence of MNZ, at room temperature

C-MNZ/ mmol L^{-1}	OCP/ mV vs. Ag/AgCl	R_s/ Ω cm^2	C_{dl}/ μF cm^{-2}	*n*	Depletion/ degree	R_{ct}/ Ω cm^2	Log*Z*/ Ω cm^2	Phase/ degree	*IE*/ %
Carbon steel									
0	-550	1.146	117.6	0.936	-13.3	20.9	1.33	-66.5	-
0.2	-550	1.132	113.1	0.939	-11.8	50.7	1.71	-60.7	58.7
0.4	-518	1.145	95.3	0.948	-5.62	73.1	1.87	-66.8	71.4
0.6	-513	1.092	70.2	0.942	-13.7	92.8	1.97	-67.3	77.4
0.8	-502	1.064	48.1	0.953	-6.83	124.8	2.1	-68.6	83.3
304L Stainless steel									
0	-434	4.32	110.3	0.933	-4.29	162.2	2.21	-71.1	-
0.2	-420	4.30	35.2	0.932	-2.37	245.5	2.39	-74.1	33.9
0.4	-414	4.26	32.6	0.949	-1.88	354.8	2.51	-75.5	54.3
0.6	-406	2.89	29.7	0.955	-0.38	398.1	2.6	-75.5	59.2
0.8	-404	2.52	27.6	0.966	-0.35	537.0	2.73	-76.1	69.8
Aluminum									
0	-1247	1.314	55.1	0.992	-4.37	28.2	1.48	-62.5	-
0.2	-1150	1.298	53.6	0.979	-1.81	42.9	1.68	-74.6	29.1
0.4	-1080	1.272	51.7	0.975	-1.13	137.8	2.21	-77.1	79.5
0.6	-968	1.236	48.3	0.987	-1.35	305.1	2.49	-79.0	90.7
0.8	-963	1.13	37.8	0.962	-1.66	342.5	2.54	-79.8	91.7

3.3. MNZ action mechanism

The metronidazole action mechanism as corrosion inhibitor for carbon steel, 304L stainless steel and aluminum in 1.0 mol L^{-1} HCl solution was discussed in agreement with adsorption basic concept that implies molecular structure (inserted in Fig. 7) of inhibitor and the assumption mentioned above in accordance with the results obtained from MNZ UV-Vis spectra recorded before and after corrosion (Fig. 7) and using the literature data support [32, 33, 40-42, 52, 59-63]. Thus, it is obvious, from the inhibitor molecular structure, that the MNZ molecules can be adsorbed on the metallic surfaces through coordinative bonds formed between the pairs of non-bonding electrons of: (a) nitrogen atom from imidazole ring; (b) oxygen atoms from $-NO_2$ and -OH groups [33]. The directly coordination of lone pairs of electrons with the *d*-vacant orbital of elements from alloy surface can take place (pure adsorption) [32, 40-42] as well as, their linkages can occur with metal cations formed by oxidation in anodic process (appearance of complexes) [33, 59]. Certain studies have reported that the adsorption of complexes on the metal surface takes place by Van der Waals bonds [40, 41, 52, 50] and this is consistent with the synergism between physisorption and chemisorption of MNZ molecules on the substrate surface. Moreover, the heterocyclic ring tendency to donate electrons to the metal surface should be considered [32]. All these possibilities must be discussed according to the nature of the corroded substrate and environment, knowing that the presence of Cl^- ions produces many changes at material/solution interface due to their adsorption followed by generation of the negative charge excess towards the solution [40, 59]. Consequently, the electrostatic interaction between the metal surface and the inhibitor protonated form must be taking into consideration [32, 33] and/or the inhibitor adsorption by "bridged chloride" [60]. Thus, a distinctive approach is needed to explain the MNZ adsorption mechanism on the surface of carbon steel, 304L stainless steel and aluminum using the UV-Vis spectra presented in Fig. 7.

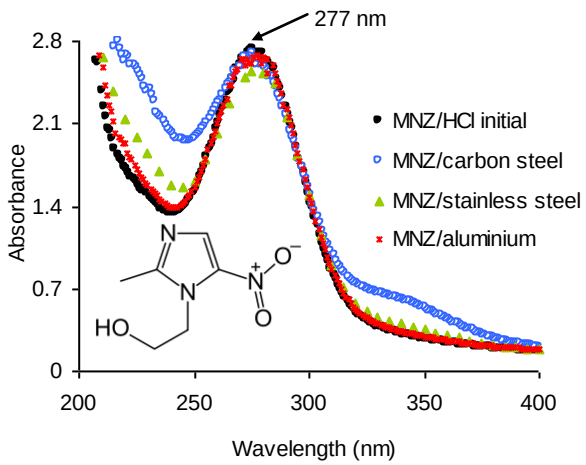

Figure 7. UV-Vis spectra recorded for: initial solution of 1.0 mol L^{-1} HCl/0.4 mmol L^{-1} MNZ; 1.0 mol L^{-1} HCl/0.4 mmol L^{-1} MNZ solution after potentiodynamic polarization performed on carbon steel, 304L stainless steel and aluminum

Farías et al. [61] identified the MNZ absorption maximum in its UV-Vis spectrum obtained in aqueous solutions, at different pH values (1.2, 3.0, 5.5 and 8.0) at 277 nm, mentioning that the MNZ protonated form is expected at pH 1.2; the protonation apparently does not affect the conjugation in the heterocyclic ring this being the main accountable for the absorption band alteration, in the UV spectrum [61]. The investigation of UV-Vis spectra illustrate in Fig. 7 leads to the conclusion that the MNZ absorption maximum at wavelength of λ_{max} = 277 nm is unchanged after the corrosion of carbon steel, 304L stainless steel and aluminum in 1.0 mol L^{-1} HCl containing inhibitor.

After MNZ interaction with the carbon steel its characteristics are strongly altered because of the formation of Fe^{2+}-MNZ complexes [32, 33, 36] by coordination between Fe^{2+} and oxygen atom from –OH group, nitrogen atom from heterocyclic ring and oxygen atom from $–NO_2$ group [33]. The parallel processes as pure adsorption and electrostatic interactions can occur, but the main responsible of the protective layer development is due to the formation of iron complexes.

The interaction of MNZ with the stainless steel leads to a slightly modification of peak characteristics, in this case a small amount of iron complexes was obtained, the MNZ anchoring on 304L stainless steel surface being favored by pure adsorption and/or electrostatic interactions. The inhibitor in contact with aluminum does not mark the peak modifications, its absorbance maximum remaining unchanged. In this case, the distribution of electrons around oxygen atoms from –OH and $–NO_2$ groups facilitates the MNZ adsorption on positive sites formed on aluminum surface during anodic process [62]; on the other hand, “bridged chloride” between MNZ molecules and aluminum surface could be formed [60].

3.4. The approach of adsorption isotherms

Overall to quantitatively express the adsorption process of the inhibitor molecules on the metal surface different adsorption isotherms were applied by fitting the degree of surface coverage (θ) values, with maximum regression coefficients. The experimental data were successfully fitted by different authors using the Langmuir [31, 37, 44-46, 49, 54, 55, 62, 64-66], Temkin [32, 41, 42, 66, 67], Frumkin [64, 66] and Freundlich [40, 53, 62, 64, 66] adsorption isotherms. Also, El-Awady and Ahmed kinetic-thermodynamic model was also applied to determine the number of occupied sites on metal surface by one inhibitor molecule [46, 49, 52, 55, 65, 67]. The degree of surface coverage (θ) was determined as *IE*/100, followed by the calculation of averages (θ_m), taking into consideration its values obtained from all performed measurements above mentioned. θ_m values were plotted depending on the MNZ concentration (*C*-MNZ), then these were fitted using a variety of functions. It was observed that the best simulation was represented by the logarithmic function (Fig. 8a), for carbon and stainless steel, when R^2 values of 0.997 and 0.985, respectively were obtained, leading to the conclusion that θ_m = f [ln(*C*-MNZ)] represents a straight line, that is according to Temkin isotherm (Eq.6).

The simulation is not characteristic for aluminum where the maximum regression coefficient (R^2) has a low value of 0.9 (Fig. 8a), which is much more distant from the unity compared to those obtained for carbon and stainless steels (0.997 and 0.985). Consequently, the θ_m graphical

representation according to ln(*C*-MNZ) will not be a straight line, this being unsuitable to fit the data corresponding to MNZ adsorption on aluminum surface, under the given experimental conditions.

Thus, in our study the best data fitting was achieved using Temkin isotherm for both carbon and stainless steel (Eq.6) [32, 41, 42, 66, 67] and El-Awady et al. kinetic-thermodynamic model for aluminum, respectively, this being indicated by Eq. 7 [46, 49, 52, 55, 65, 67].

$$\theta_{\mathrm{m}} = \frac{1}{f} \cdot \ln K + \frac{1}{f} \cdot \ln C \qquad (6)$$

$$\ln\left(\frac{\theta_{\mathrm{m}}}{1-\theta_{\mathrm{m}}}\right) = \frac{1}{n}\ln K + \frac{1}{n}\ln C \qquad (7)$$

where C is the MNZ concentration (M) in the bulk electrolyte, θ_{m} is the average value of degree of surface coverage, K is the adsorption-desorption equilibrium constant and f, $1/n$ are the heterogeneous factors of the metal surface, representing the number of surface active sites occupied by one inhibitor molecule.

By applying the Temkin isotherm for carbon steel and 304L stainless steel, the straight lines were obtained (Fig. 8b) with regression coefficient (R^2) values of 0.997 and 0.985, respectively, these being very close to unity, showing the validity of this model for the adsorption of MNZ molecules on both steels. The slopes of lines graphically represented in Fig. 8b are equal with $1/f$ and the intercepts from which the K values were calculated are represented by $[(1/f)\cdot\ln K]$.

In contrast, for aluminium, the El-Awady kinetic-thermodynamic model [46, 49, 52, 55, 65, 67] fitted better the experimental data, R^2 reaching a value of about 0.97. Through graphically representation of $\ln[\theta_{\mathrm{m}}/(1-\theta_{\mathrm{m}})]$ as a function of ln(C-MNZ), a straight line was obtained (Fig. 8c), with the slope defined by $1/n$ and the intersection with the ordinate being expressed by $[(1/n)\cdot\ln K]$.

The thermodynamic parameters for the adsorption molecules of MNZ on carbon steel, 304L stainless steel and aluminum in 1.0 mol L^{-1} HCl solution, at room temperature are shown in Table 3.

The Eq. 8 was used to calculate the standard adsorption free energy ($\Delta G^{o}_{\mathrm{ads}}$) [31, 32, 37, 30-42, 44-46, 49, 52-55, 62, 64-67]:

$$\Delta G^{o}_{\mathrm{ads}} = R\cdot T\,[\ln(1/55.5) - \ln K] \qquad (8)$$

where R is the universal constant of gases (8.31 J mol^{-1} K^{-1}), T is the temperature (298 K) and *55.5* is the value of the molar concentration of water in the solution

As shown the Table 3, the number that indicates the occupied active surface sites by one MNZ molecule is different. This suggests that the MNZ adsorption mechanism involves many aspects depending on: (i) the changes occurred at material/electrolyte interface; (ii) the content or type of ions and their distribution in the electric double layer; (iii) type of bonds which facilitate the MNZ adsorption on the metal surfaces. As shown, the MNZ molecule, has an excess of negative charge resulted from the local concentration of electrons at oxygen atoms from the $-NO_2$ and –OH groups, around the two nitrogen atoms of the imidazole ring, as well as an uniform distribution of electrons inside of the heterocyclic ring. Thus, those five active sites occupied by one inhibitor molecule on carbon steel surface can justify the formation of complexes of MNZ with Fe^{2+} as a primary process, prevailing the pure adsorption or the adsorption of the MNZ protonated form.

This is supported by the $\Delta G^{o}_{\mathrm{ads}}$ value of -38.4 kJ mol^{-1} indicating a spontaneous adsorption *via* the mixed mechanism of physisorption and predominant chemisorption, this being very close to -40 kJ

mol^{-1} that is generally considered as a limit between chemical and physical adsorption [31, 32, 37, 39-42, 44-46, 49, 52-55, 62, 64-67].

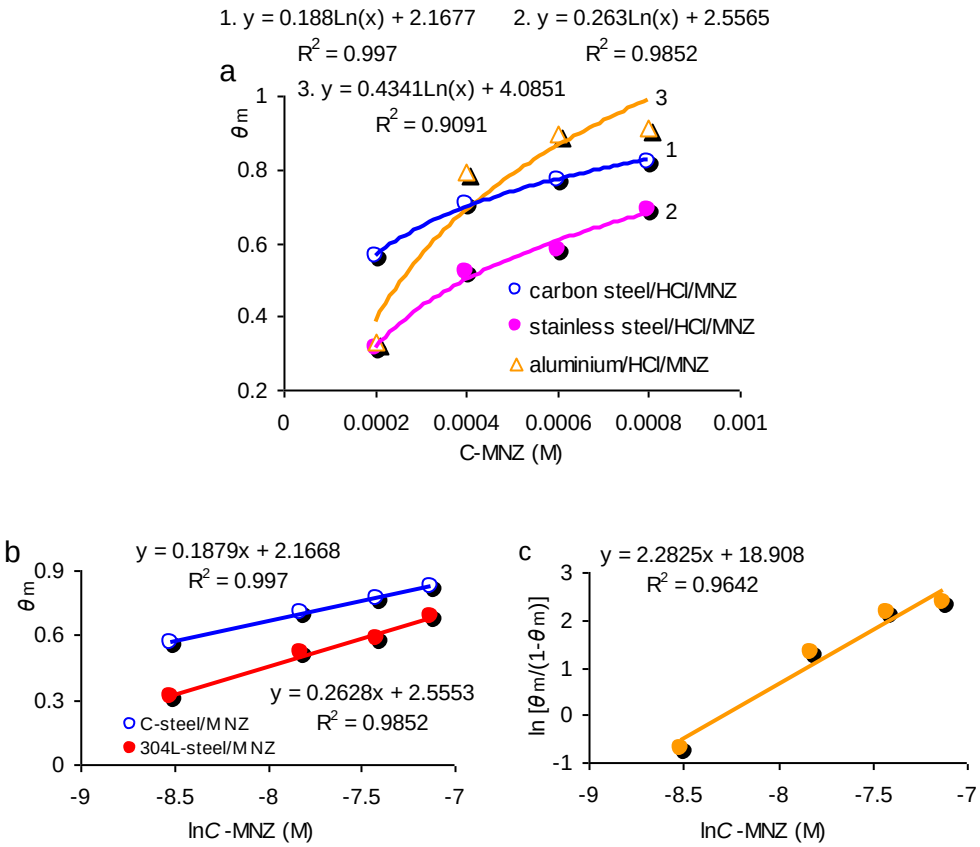

Figure 8. Simulation of average values (θ_m) over metronidazole concentration (a); Temkin diagram obtained for carbon steel and 304L stainless steel corroded in 1.0 mol L^{-1} HCl solution containing various MNZ concentrations (b); Kinetic-thermodynamic model of El-Awady applied for aluminum corrosion in 1.0 mol L^{-1} HCl solution in the presence of various MNZ concentrations (c)

Table 3. Thermodynamic parameters for the MNZ adsorption on carbon steel, 304L stainless steel and aluminum in 1.0 mol L^{-1} HCl solution, at room temperature

Temkin adsorption isotherm			
slope	f	ln K	ΔG^o_{ads} (kJ mol^{-1})
Carbon steel			
0.1879	5.3	11.5	-38.4
304L Stainless steel			
0.2628	3.8	9.7	-34.0
Kinetic- thermodynamic model of El-Awady and Ahmed			
n	1/n	lnK	ΔG^o_{ads} (kJ mol^{-1})
Aluminum			
0.438	2.3	8.3	-30.5

Compared to the previous case, ΔG^{o}_{ads} for stainless steel has a lower value of -34.0 kJ mol^{-1}, attesting the formation of a protective film by a mechanism of moderate chemical adsorption [41, 68] on the surface observing that, one molecule of inhibitor occupies approximately four active sites (versus five), probably, this is due to a competitive process of surface passivation followed by a oxide film appearance that blocks certain active areas [37]. The performance of MNZ for corrosion of carbon steel is higher than that was obtained for 304L stainless steel, this being strongly sustained by its action mechanism above discussed. Instead, the ΔG^{o}_{ads} value of -30.5 kJ mol^{-1} determined for aluminum certifies a closer mechanism of physical adsorption when two active sites were blocked by one molecule of MNZ. In this case, the synergic effect between the electrostatically adsorption and the donation of electrons from inhibitor to aluminum surface takes place [66]. For a short time the MNZ performance as corrosion inhibitor for aluminum is better than that obtained for carbon steel, but a long time, the inhibitor desorption from the surface is inevitable, because the protective layer is anchored by weaker bonds which can easier cleave than the coordinative bonds.

4. CONCLUSIONS

The performance of metronidazole as corrosion inhibitor for carbon steel, 304L stainless steel and aluminum in 1.0 mol L^{-1} HCl solution was tested by potentiodynamic polarization and electrochemical impedance spectroscopy (EIS), in order to discuss comparatively the electrochemical parameters and the mechanism of the protective layer formation. The UV-Vis spectrophotometry was used as an associative method for the analysis of 1.0 mol L^{-1} HCl solution, without and with MNZ, before and after corrosion to detect their composition changes.

The data corroboration leads to the conclusion that MNZ behaves as corrosion inhibitor reaching the maximum inhibition efficiency of 90.5±1.5% for aluminum, the level of 82.0±1.0% for carbon steel and finally, 68.8±1.0% for 304L stainless steel.

The action mechanism of metronidazole as corrosion inhibitor of carbon steel, 304L stainless steel and aluminum in 1.0 mol L^{-1} HCl solution was discussed by corroboration the data obtained from electrochemical measurements with the UV-Vis spectrophotometry results, concluding that, the protective layer composition depends on the surface chemistry and type of bonds which bind the inhibitor on substrate.

The experimental data were fitted using Temkin adsorption isotherm for carbon steel and 304L stainless steel that indicated a moderate adsorption of MNZ molecules on carbon steel surface. This involves both chemical and physical adsorption mechanism, due to: interactions between the non-bonding electrons of the nitrogen and oxygen atoms with the vacant "*d*" orbital of the elements from the metal network and/or coordination with Fe^{2+} ions forming complexes anchored *via* Van der Waals bonds, the latter being the main MNZ action mechanism in the case of carbon steel. The adsorption mechanism of MNZ on aluminum surface supported by Awady kinetic model is the result of the synergic effect between the electrostatically interaction and the donation of electrons from inhibitor to aluminum surface.

The occurrence of another competitive process like surface passivation by oxide film formation leads to the decreases of the number of active sites which are blocked by one molecule of inhibitor,

and consequently the MNZ performance is lower for 304L stainless steel compared to that obtained for carbon steel.

Moreover, high performance of MNZ for aluminum corrosion inhibition in 1.0 mol L^{-1} HCl solution is temporary valid, the protective layer could be degraded because of the inhibitor desorption facilitated by a physical adsorption mechanism.

References

1. L. Larabi, Y. Harek, M. Traisnel and A. Mansri, *J. Appl. Electrochem.,* 34 (2004) 833.
2. A. Samide, E. Turcanu and I. Bibicu, *Chem. Eng. Commun.,* 196 (2009) 1008.
3. H. Ashassi-Sorkhabi, Z. Ghasemi and D. Seifzadeh, *Appl. Surf. Sci.,* 249 (2005) 408.
4. A. Subramania, N. T. K. Sundaram, R. S. Priya, K. Saminathan, V. S. Muralidharan and T. Vasudevan, *J. App. Electrochem.,* 34 (2004) 693.
5. S. S. A. El-Rehim, S. A. M. Refaey, F. Taha, M. B. Saleh and R. A. Ahmed, *J. Appl. Electrochem.,* 31 (2001) 429.
6. A. Samide, I. Bibicu, M. Rogalsky and M. Preda, *Corros. Sci.,* 47 (2005) 1119.
7. M. A. Quraishi, F. A. Ansari and D. Jamal, *Mater. Chem. Phys.,* 77 (2003) 687.
8. N. Hassan and R. Holze, *J. Chem. Sci*., 121 (2009) 693.
9. A. Samide, B. Tutunaru, C. Negrila, I. Trandafir and A. Maxut, *Dig. J. Nanomater. Bios.,* 6 (2011) 663.
10. K. F. Khaled and N. Hackerman, *Electrochim. Acta,* 48 (2003) 2715.
11. I. Forsal, L. Lakhrissi, K. Naji, S. Abirou, M. E. Touhami, B. Lakhrissi and M. Addou, *Spectrosc. Lett.,* 43 (2010) 136.
12. I. B. Obot and N. O. Obi Egbedi, *Corros. Sci.,* 52 (2010) 198.
13. N. O. Eddy, U. J. Ibok, E. E. Ebenso, A. El Nemr and E. S. H. El Ashry, *J. Mol. Mod.,* 15 (2009) 1085.
14. M. Abdallah, *Corros. Sci.,* 46 (2004) 1981.
15. S. K. Shukla and M. A. Quraishi, *Mater. Chem. Phys.,* 120 (2010) 142.
16. X. H. Pang, W. J. Guo, W. H. Li, J. D. Xie and B. R. Hou, *Sci. China Ser. B-Chem.,* 51 (2008) 928.
17. X. Pang, X. Ran, F. Kuang, J. Xie and B. Hou, *Chinese J. Chem. Eng.,* 18 (2010) 337.
18. S. K. Shukla and M. A. Quraishi, *Corros. Sci.,* 52 (2010) 314.
19. N. O. Eddy, S. A. Odoemelam, E. C. Ogoko and B. I. Ita, *Port. Electrochim. Acta,* 28 (2010) 15.
20. A. S. Fouda, W. M. Abo-Elmeaty and H. M. El-Abbasy, *Zastita Materijala* (*Materials Protection*), 50 (2009) 3.
21. H. Ashassi-Sorkhabi, B. Shabani, B. Aligholipour and D. Seifzadeh**,** *Appl. Surf. Sci.,* 252 (2006) 4039.
22. M. M. El-Naggar, *Corros. Sci.,* 49 (2007) 2226.
23. T. Arslan, F. Kandemirli, E. E. Ebenso, I. Love and H. Alemu, *Corros. Sci.,* 51 (2009) 35.
24. S.K. Shukla, A.K. Singh, I. Ahamad and M.A. Quraishi, *Mater. Lett*., 63 (2009) 819.
25. M. Abdallah, *Corros. Sci*., 44 (2002) 717.
26. N. F. Atta, A. M. Fekry and H. M. Hassaneen, *Int. J. Hydrogen Energ.,* 36 (2011) 6462.
27. S. M. Tamborim, S. L. P. Dias, S. N. Silva, L. F. P. Dick and D. S. Azambuja, *Corros. Sci.,* 53 (2011) 1571.
28. A. S. Fouda, A. A. Al-Sarawy, F. Sh. Ahmed and H. M. El-Abbasy, *Corros. Sci.,* 51 (2009) 485.
29. A. S. Fouda, G. Y. El-Ewady and K. Shalabi, *J. Korean Chem. Soc.,* 55 (2011) 268.
30. I. B. Obot, N. O. Obi-Egbedi, S. A. Umoren and E. E. Ebenso, *Chem. Eng. Commun.,* 198 (2011) 711.
31. B. Zerga. A. Attayibat, M. Sfaira, M. Taleb, B. Hammouti, M. Ebn Touhami, S. Radi and Z. Rais, *J. Appl. Electrochem.,* 40 (2010) 1575.

32. I. B. Obot, E. E. Ebenso and M.M. Kabanda, *J. Environ. Chem. Eng.,* 10 (2013) 431.
33. S. M. Megalai, P. Manjula, K. N. Manonmani, C. N. Kavitha and N. Babyd, *Port. Electrochim. Acta,* 30 (2012) 395.
34. M. Sobhi, *Prot. Met. Phys. Chem. Surf.,* 50 (2014) 825.
35. F. Siraji, A. T. M. Z. Azam, M. S. Amran, J. N. Islam, F. M. Amjad and M. A. Hossain, *J. Sci. Res.,* 4 (2012) 173.
36. J. A. Obaleye and A. Lawal, *J. Appl. Sci. Environ. Manage.,* 11 (2007) 15.
37. M. Scendo and J. Trela, *Int. J. Electrochem. Sci*., 8 (2013) 9201.
38. J. Halambek, A. Zutinic and K. Berkovic, *Int. J. Electrochem. Sci.,* 8 (2013) 11201.
39. R. S. Abdel Hameed, E. A. Ismaif, A. H. Abu-Nawwal Hussin and I. AL-Shafey, *Int. J. Electrochem. Sci.,* 10 (2015) 2098.
40. A. Samide, B. Tutunaru, C. Ionescu, P. Rotaru and L. Simoiu, *J. Therm. Anal. Calorim.,* 118 (2014) 631.
41. A. Samide, P. Rotaru, C. Ionescu, B. Tutunaru, A. Moanţă and V. Barragan-Montero, *J. Therm. Anal. Calorim.,* 118 (2014) 651.
42. A. Samide and B. Tutunaru, *Cent. Eur. J. Chem.,* 12 (2014) 901.
43. Y. H. Ahmad and W. M. I. Hassan, *Int. J. Electrochem. Sci.,* 7 (2012) 12456.
44. N. Ca1iskan and E. Akbas, *Mater. Chem. Phys.,* 126 (2011) 983.
45. M. Abdalla, I. Zaasfarany, S. O. Al-Karanee and A. A. Abd El-Fattah, *Arab. J. Chem.,* 5 (2012) 225.
46. A. S. Fouda, H. A. Mostafa and H.M. El-Abbasy, *J. Appl. Electrochem.,* 40 (2010) 163.
47. X. Li, S. Den and H. Fu, *Corros., Sci.,* 53 (2011) 1529.
48. H. I. Al-Shafey, R. S. Abdel Hameed, F. A. Ali, Abd El-Aieem S. Aboui-Magd and M. Salah, *Int. J. Pharm. Sci. Rev. Res.,* 27 (2014) 146.
49. A. A. Nazeer, H. M. El-Abbasy and A. S. Fouda, *Res. Chem. Intermediat.,* 39 (2013) 921.
50. Gh. Golestani, M. Shahidi and D. Ghazanfari, *Appl. Surf. Sci.,* 308 (2014) 347.
51. R. S. Dubey and Y. Potdar, *Indian J. Chem. Techn.,* 16 (2009) 334.
52. A. S. Fouda and H. M. El-Abbasy, *Corrosion,* 68 (2012) A1-A9.
53. M. Abdallah and B. A. AL Jahdaly, *Int. J. Electrochem. Sci.,* 10 (2015) 9808.
54. J. I. Bhat, and V. D. P. Alva, *Trans. Indian Inst. Met.,* 64 (2011) 377.
55. A. A. Nazeer, H. M. B-Abbasy and A. S. Fouda, *J. Mater. Eng. Perform.,* 22 (2013) 2314.
56. M. N. EI-Haddad and K. M. Elattar, *Int. J. Ind. Chem.,* 6 (2015) 105.
57. M. Shahidi, E. Sasaei, M. Ganjehkaviri and M. R. Gholamhosseinzadeh, *J. Phys. Theor. Chem.,* 9 (2012) 149.
58. M. Bobina, A. Kellenberger, J. P. Millet, C. Muntean and N. Vaszilcsin, *Corros. Sci.,* 69 (2013) 389.
59. M. E. Ikpi, I. I. Udoh, P. C. Okafor, U. J. Ekpe and E. E. Ebenso, *Int. J. Electrochem. Sci.,* 7 (2012) 12193.
60. M. I. Awad, *J. Appl. Electrochem.,* 36 (2006) 1163.
61. T. Farías, A. R. Ruiz-Salvador and A. Rivera, *Micropor. Mesopor. Mat.,* 61 (2003) 117.
62. R. M. Hassan, and I. A. Zaafarany, *Materials,* 6 (2013) 2436.
63. A. Samide, B. Tutunaru, A. Dobrițescu, P. Ilea, A. C. Vladu and C. Tigae, *Int. J. Electrochem. Sci.,* 11 (2016) 5520.
64. B. Zerga, B. Hammouti, M. Ebn Touhami, R. Touir, M. Taleb, M. Sfaira, M. Bennajeh and I. Forssal, *Int. J. Electrochem. Sci.,* 7 (2012) 471.
65. M. Abdallah, I. Zaafarany, J. H. Al-Fahemi, Y. Abdallah and A. S. Fouda, *Int. J. Electrochem. Sci.,* 7 (2012) 6622.
66. I. B. Obot, N. O. Obi-Egbedi and S. A. Umoren, *Corros. Sci.,* 51 (2009) 1868.
67. M. Abdallah, I. Zaafarany, A. Fawzy, *M. A.* Radwan and E. Abdfattah, *J. Am. Sci.,* 9 (2013) 580.

68. A. Samide, B. Tutunaru, A. Moanţă, C. Ionescu, C. Tigae and A. C. Vladu, *Int. J. Electrochem. Sci.*, 10 (2015) 4637.

© 2017 The Authors. Published by ESG (www.electrochemsci.org). This article is an open access article distributed under the terms and conditions of the Creative Commons Attribution license (http://creativecommons.org/licenses/by/4.0/).